The roles of temperature and water vapor at different stages of the polar mesospheric cloud season

P. P. Rong,[1] J. M. Russell III,[1] M. E. Hervig,[2] and S. M. Bailey[3]

Received 24 June 2011; revised 16 December 2011; accepted 19 December 2011; published 23 February 2012.

[1] Temperature, or alternatively, saturation vapor pressure (P_{SAT}), dominantly controls the polar mesospheric cloud (PMC) seasonal onset and termination, characterized by a strong anticorrelated relationship between the Solar Occultation for Ice Experiment (SOFIE)-observed PMC frequency and P_{SAT} on intraseasonal time scales. SOFIE is highly sensitive to weak clouds and can obtain a nearly full spectrum of PMCs. Both the SOFIE PMC frequency and P_{SAT} indicate a rapid onset and termination of the season. Compared to P_{SAT}, the water vapor partial pressure (P_{H2O}) exhibits only a slight increase from before to after the start of the season. We are able to use the P_{SAT} daily minimum and two averaged P_{H2O} levels taken before and after the solstice, respectively, to estimate the start and end days of the PMC season within 1–2 days uncertainty. SOFIE ice mass density and its relationship to P_{H2O} and P_{SAT} are examined on intraseasonal scales and for two extreme conditions, i.e., strong and weak cloud cases. In the strong cloud case, such as those bright clouds that occur during the core of the season, P_{H2O} far exceeds P_{SAT} and dominantly controls the ice mass density variation, while in the weak cloud case, such as those clouds that occur at the start and end of the season, P_{H2O} and P_{SAT} have comparable magnitudes, vary in concert, and have similar effects on the ice mass density variation. These results suggest that the long-term brightness trends reported by DeLand et al. (2007) are primarily driven by changes in water vapor (H_2O), not temperature.

Citation: Rong, P. P., J. M. Russell III, M. E. Hervig, and S. M. Bailey (2012), The roles of temperature and water vapor at different stages of the polar mesospheric cloud season, *J. Geophys. Res.*, *117*, D04208, doi:10.1029/2011JD016464.

1. Introduction

[2] Polar mesospheric clouds (PMCs), also called noctilucent clouds (NLCs) when observed from the ground, form under the prevailing conditions of a cold mesopause (e.g., <150 K) and enhanced mesospheric water vapor (H_2O) in the high-latitude summer (poleward of 60°) [e.g., *Garcia and Solomon*, 1985]. Accordingly a low saturation vapor pressure (e.g., $P_{SAT} < 1.0 \times 10^{-8}$ hPa) and relatively high water vapor partial pressure ($P_{H2O} > 1.0 \times 10^{-8}$ hPa) coexist. When summer starts, P_{SAT}, which is predominantly dependent on $e^{-1/T}$, drops rapidly as T decreases in the summer mesosphere. Meanwhile, P_{H2O} experiences a moderate increase that is caused by the upward transport of H_2O from the wetter lower atmosphere. Both occurrences contribute to achieve a supersaturated state ($S > 1$, where $S = P_{H2O}/P_{SAT}$) and are linked to a global scale mesospheric residual circulation that has an upwelling branch in the polar summer mesosphere [*Garcia and Solomon*, 1985]. As a prominent seasonal phenomenon, PMC variability on a series of time scales, for example, hourly to daily, intraseasonal, interannual, and decadal, has attracted intense research interest over the years. It has been difficult to readily obtain PMC variability on all desired time scales because historically the PMC/NLC measurements lack temporal continuity and also are sparse in spatial coverage. Despite such a limitation, using a collection of NLC observations since 1964 in northwest Europe (~54–61°N), *Gadsden* [1998a] performed a comprehensive study on the secular change of NLC brightness, frequency, southern edge, seasonal length, and preferred local time of appearance. It was concluded that after removing the solar cycle modulation there is an upward trend in the NLC frequency, while other aspects of the morphology remained fairly constant over the years. For example, there is no apparent brightness increase, and the length of the season also remained unchanged over the years. However, there are other studies that yield different conclusions on the long-term trend of the NLC frequency. For example, *Kirkwood and Stebel* [2003] analyzed the NLC appearance frequency in part of northern Europe and did not find any notable trend for the last 40 years [also see *Thomas*, 2003]. Consistent with this finding, an analysis of the NLCs in Moscow for the last 40 years also indicated that there was no apparent long-term trend in the cloud frequency [*Romejko et al.*, 2003]. Results of *Romejko et al.* [2003] did however imply a slight upward trend in the cloud brightness. Using the SBUV series of satellites data sets, *Shettle et al.* [2009] found an upward

[1]Center for Atmospheric Sciences, Hampton University, Hampton, Virginia, USA.
[2]GATS, Inc., Driggs, Idaho, USA.
[3]Bradley Department of Electrical and Computer Engineering, Virginia Polytechnic Institute and State University, Blacksburg, Virginia, USA.

0148-0227/12/2011JD016464

trend in the PMC frequency for the last 30 years since 1979, which is consistent with the SBUV cloud brightness trend found by *DeLand et al.* [2007]. Determination of the cloud frequency or brightness trends can be affected by a number of factors such as, data sampling techniques, local time (LT), latitude, and the brightness threshold used in the cloud detection [*Stevens et al.*, 2007]. For example, the conclusions drawn from analyzing the SBUV data sets may have been affected by the fact that the SBUV instruments only detect bright clouds. To diagnose whether the long-term trend or any other PMC variability is properly determined, we must understand the mechanisms that control the cloud frequency and brightness.

[3] It is well known that temperature and H_2O are two key factors that control the PMC formation and variation, and this subject has been extensively studied through model simulations. Within a well-established theoretical framework a number of PMC models were proposed to study how temperature, H_2O, and other factors such as nucleation and dynamics control PMC formation and variation [e.g., *Jensen and Thomas*, 1988; *Gadsden*, 1998b; *von Zahn and Berger*, 2003; *Lübken et al.*, 2007; *Hervig et al.*, 2009b], but unequivocal observational evidence has, up to now, been lacking. The SOFIE data set can serve to provide such evidence and to better define our understanding of the roles of temperature and H_2O in controlling PMCs.

[4] The Solar Occultation for Ice Experiment (SOFIE) aboard the Aeronomy of Ice in the Mesosphere (AIM) satellite (2007–present) [*Russell et al.*, 2009] measures PMCs, temperature, and H_2O simultaneously on fine vertical grids, which provides a better opportunity to clarify how temperature and H_2O control PMCs than existing and past satellites. First, SOFIE can detect weak clouds, including the faintest ice layers [*Hervig et al.*, 2009a]. This capability is essential in studying the existence of PMCs. The high sensitivity of SOFIE is related to its high signal-to-noise ratio ($\sim 10^6$ at $\sim$83 km). Although higher signal-to-noise ratio is a known advantage of the solar occultation technique, the band pairs used in SOFIE further reduces the noise level [*Gordley et al.*, 2009]. Second, SOFIE measurements have high vertical resolution. SOFIE measures all parameters with a $\sim$2 km vertical resolution throughout its altitude range ($\sim$15–100 km). The high vertical resolution makes the PMCs and the corresponding temperature and H_2O more precisely matched so that the correlation between the PMCs and their environmental variables can be readily obtained. Third, SOFIE measurement latitude remains poleward of 65°, and therefore a continuous intraseasonal time series can be obtained in a polar regional averaged sense. Nevertheless, since the SOFIE measurement latitude varies significantly throughout the PMC season we must consider the possible effect of this latitude migration on the results. Last, SOFIE infrared observations are a direct measure of ice mass density. Accordingly, a macrophysical relationship with the environmental variables can be obtained without the necessity of looking into the microphysics.

[5] This paper investigates how temperature and H_2O control the PMC existence and strength on intraseasonal scales using the SOFIE measured PMCs, temperature, and H_2O, and a 0-D model proposed by *Hervig et al.* [2009b]. Only the Northern Hemisphere (NH) clouds are examined in this study because they exhibit less variability and their controlling mechanisms are presumably less complex than their southern counterpart [e.g., *Gumbel and Karlsson*, 2011]. We present two main parts of research in this paper. In part one we use the PMC daily occurrence frequency to examine what controls the start and end of the PMC season; in part two we examine what controls the PMC ice mass density variation during the core of the cloud season. In the analysis of the cloud seasonal start and end, the Microwave Limb Sounder (MLS) [*Waters et al.*, 2006] temperature and H_2O are also used to support the SOFIE results. The 0-D model results are used in both parts of the analysis to compare with the SOFIE observations. The 0-D model assumes that ice forms as long as the supersaturation ratio (S) is greater than one and that H_2O in excess of P_{SAT} exists as ice. In the 0-D model the nucleation processes and the effect from the atmospheric flow field are ignored. Although highly simplified, the 0-D model has proven to be effective in revealing PMC variations on intraseasonal scales [*Hervig et al.*, 2009b; *Russell et al.*, 2010]. Instead of directly addressing temperature and H_2O we use P_{SAT} and P_{H2O} as intermediate variables to reflect the temperature and H_2O in this study. The P_{SAT} and P_{H2O} are chosen because their relationship with the equilibrium ice mass density is quasi-linear, and because the P_{SAT} variation can be used to effectively interpret the rapid onset and termination of the PMC season.

2. Data Sets and 0-D Model

2.1. SOFIE Level2 Temperature, H_2O, and PMC Data Sets

[6] SOFIE is one of the two instruments that are operating aboard the AIM satellite [*Russell et al.*, 2009], and it has been collecting scientific data since 14 May 2007. The publically released level2 data began on 28 May 2007. SOFIE measures the atmospheric limb transmission using eight channels centered between 0.292 μm and 5.316 μm. Each channel consists of two broadband radiometer measurements, one in a strong absorption band, and the other in a spectrally adjacent region of weak absorption [*Gordley et al.*, 2009]. SOFIE level2 products include temperature, O_3, H_2O, CO_2, CH_4, and NO. Although the vertical range of SOFIE level2 products is $\sim$15–100 km, the altitude range with the highest data quality is in the mesosphere. As was mentioned above, the vertical resolution of SOFIE remains at $\sim$2 km for all of its retrieved products. The horizontal resolution corresponding to the vertical field of view at $\sim$83 km along the tangent path and about $\sim$7 km perpendicular to the path. SOFIE temperature is retrieved from the two CO_2 channels, channel 4 (2.785 and 2.939 μm) and channel 7 (4.324 and 4.646 μm). The H_2O product is retrieved from channel 3 (2.462 μm and 2.618 μm) signals. The level 2 SOFIE H_2O throughout the upper stratosphere and mesosphere has been validated by *Rong et al.* [2010], and has been shown to have high precision and accuracy based on the analysis of its instrument properties and the comparisons with ACE/Sci-Sat1 (Atmospheric Chemistry Experiment) [*Bernath et al.*, 2005] and MLS/Aura measured H_2O [*Lambert et al.*, 2007]. The SOFIE H_2O random error is $\sim$0.25–1.0% below $\sim$85 km, which is the highest among the currently existing mesospheric data

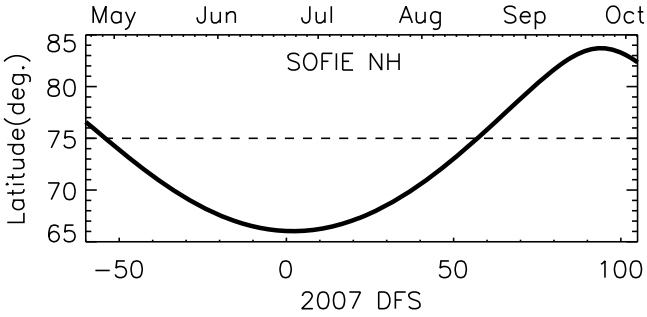

Figure 1. SOFIE Northern Hemisphere (NH) latitude coverage during summer and early fall. SOFIE latitude coverage repeats every 6 months. The horizontal axis is days from summer solstice (DFS).

sets. The SOFIE H_2O systematic error is within ∼3–12% below ∼85 km, as compared to the ∼9–34% systematic error of MLS H_2O for the same altitude range. SOFIE H_2O in the NH shows overall excellent agreement (∼2–5% mean percent difference) with both ACE and MLS data except for differences caused by the enhancement layer at ∼80–82 km. This layer is formed at the bottom of the PMC region due to recycling of H_2O from the ice to vapor form [*Summers et al.*, 2001]. SOFIE detects this feature more distinctly owing to its high vertical resolution. The high resolution also enables a more precise determination of the mesopause and leads to serendipitous findings in the seasonal development of the mesopause region, such as, a double-mesopause detected at the end of the summer (see section 3.3). A sequence of temperature validation studies were conducted at different stages of data release and a paper describing these results has been written and will be submitted in the near future (M. H. Stevens et al., Validation of upper mesospheric and lower thermospheric temperatures measured by the solar occultation for ice experiment, manuscript in preparation, 2012). These unpublished studies indicate that in the NH polar summer mesosphere for near-coincident locations and timeframes (1° in latitude and 1 h in time) the SOFIE temperature agrees well with Sounding of the Atmosphere using Broadband Emission Radiometer aboard the TIMED satellite (SABER/TIMED) [*Russell et al.*, 1999; *Remsberg et al.*, 2008] and ACE/Sci-Sat1 [*Sica et al.*, 2008] measurements, with the mean differences being ∼2–5 K. Especially at the mesopause there is no cold or warm bias shown in these comparisons based on the coincidences. However, the average of all events north of 65°N suggests a few degrees warmer mesopause region in SOFIE than in SABER. This is because SOFIE did not capture some very low temperatures (<130 K at mesopause) that are present in SABER [*Russell et al.*, 2010]. When compared to the falling sphere measurements [*Lübken et al.*, 1996], the SOFIE mesopause is warmer by ∼15–20 K and lower in height based on the comparisons of SABER and falling sphere climatology shown in the work of *Remsberg et al.* [2008].

[7] SOFIE channels 2 and 5 are dedicated to PMC measurements. *Hervig et al.* [2009a] described detailed theoretical frameworks and algorithms for the retrieval of several key PMC variables such as ice mass density, ice particle number density, ice particle axial ratio, effective radius, PMC top and bottom heights, and the height where maximum ice mass density occurs (Z_{max}, also called cloud peak height hereinafter).

2.2. MLS Level2 Temperature and Water Vapor

[8] MLS/Aura level2 temperature [*Schwartz et al.*, 2008] and H_2O [*Lambert et al.*, 2007] are used to conduct parallel analyses to verify the SOFIE results. The MLS temperature and H_2O vertical resolutions degrade to 14–16 km in the mesopause region and therefore the mesopause height cannot be precisely determined. In this case simply the coldest mesospheric temperature is taken as the mesopause temperature to compare with the SOFIE results. The coarser vertical resolution of MLS is not a problem in this study because mesopause height is not essential in our analyses.

2.3. SOFIE Latitudes and Local Times

[9] Prior to the main analysis we first address two major considerations that should be taken into account when interpreting the results of the analysis. The first consideration is the SOFIE latitude migration throughout the PMC season shown in Figure 1. From mid-May to late August the SOFIE latitude varies between ∼66° and ∼80°; before and after the summer solstice, SOFIE measurements extend into lower and higher latitudes, respectively. Temperature is known to exhibit a significant latitudinal gradient in the polar summer mesopause region, i.e., a ∼10 K decrease on average from 66° to 80° around the summer solstice [e.g., *Garcia and Solomon*, 1985]. This can affect the cloud frequency in the core of the season. However, the temperature gradient is generally smaller at the start and end than in the middle of the summer. In particular, the onset and termination of the PMC season will not be significantly affected. This will be discussed further in a following section. Water vapor (e.g., volume mixing ratio) shows an overall less distinct latitudinal gradient, and therefore less impact is expected from the latitude change.

[10] Local time (LT) variation is another consideration. SOFIE always measures the NH at the local sunset time (2200–2300 LT) while the chosen MLS data points experience a wider range of local time variation, i.e., typically from about 0200 LT to 1300 LT. *Stevens et al.* [2010] suggested that the polar summer mesosphere temperature at 69°N in June varies with LT and the magnitude reaches ∼8 K around the mesopause. On the basis of their results, SOFIE and MLS LTs are in the warm and cold periods of the diurnal cycle, respectively, and this could lead to a temperature bias between the two data sets and accordingly could have some effect on the 0-D model determined start and end of the PMC season.

2.4. The 0-D Model

[11] The 0-D model [*Hervig et al.*, 2009b] assumes that all H_2O in excess of saturation is instantaneously transferred into the ice phase. Although highly simplified, the 0-D model is a suitable framework to describe PMC variations in a developed stage. More specifically, the 0-D model has been shown to be useful in revealing PMC variations with time scales longer than a day. Many previous modeling studies [e.g., *Jensen and Thomas*, 1988; *Rapp and Thomas*, 2006] have suggested that it takes about a few hours to a day for PMCs to form and grow into a mature stage in which there is

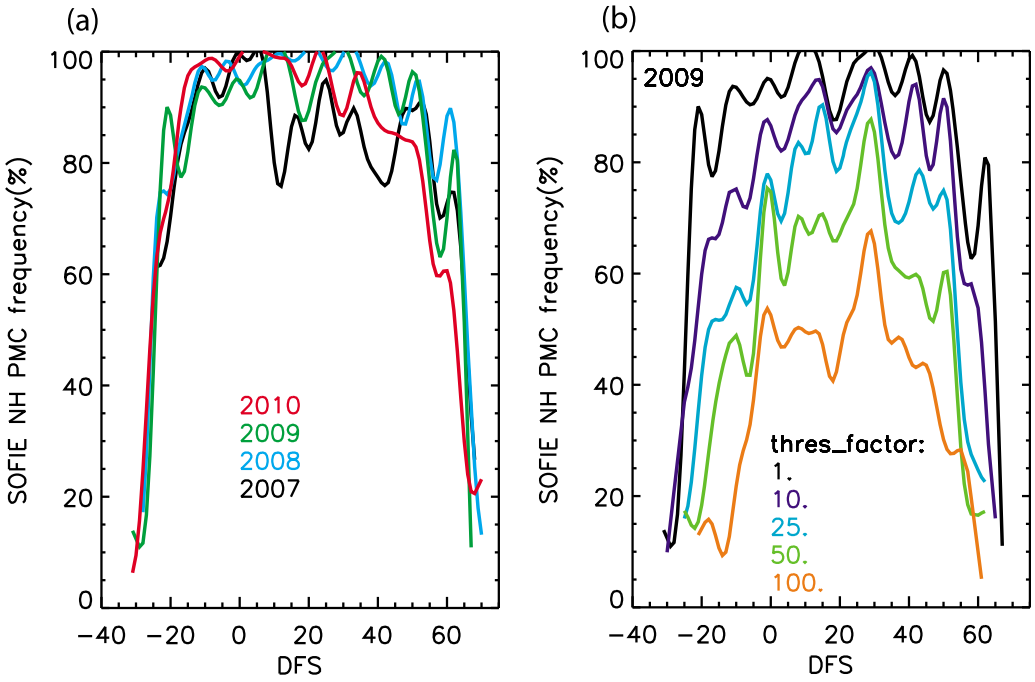

Figure 2. (a) SOFIE observed daily PMC frequency for four consecutive NH seasons. (b) SOFIE PMC daily frequency variations based on a series of different threshold ice mass density values, which are 5, 10, 25, 50, and 100 times of the default threshold, i.e., 0.15 ng/m^3, respectively.

a strong freeze-dried region below the clouds and near-steady Z_{max} and ice mass density. Since the PMC measurements are mostly taken at the developed stage of the clouds, the results of the 0-D model can agree well with the observations. For example, *Russell et al.* [2010] has shown that the daily averaged difference of cloud height and mesopause height remains at ~3.5 km throughout the entire PMC season, and this height difference can be well reproduced by the 0-D model. In the 0-D model a given temperature vertical profile and the corresponding H_2O profile are used to produce one ice mass density profile. Since the fall velocity and vertical transport are ignored, the ice mass density peak height is the altitude where the H_2O in excess of the saturation value (i.e., S > 1) is the largest, which is generally 3.5 km below the mesopause. This indicates that on a daily scale the fall velocity and vertical transport has little effect on adjusting the peak cloud height up or down. The P_{SAT} formula used in the 0-D model is from *Murphy and Koop* [2005], written as:

$$P_{SAT} = e^{9.550426-\frac{5723.265}{T}+3.53068\cdot\log(T)-0.00728332\cdot T}/100(hPa) \quad (1)$$

The 0-D ice mass density is written as:

$$m_{ice}(P_{H2O}, P_{SAT}) = (P_{H2O} - P_{SAT})\cdot 100\cdot 10^{-6} \cdot 10^{9}\cdot Mww/R/T\ (ng/m^3) \quad (2)$$

where $m_{ice}(P_{H2O}, P_{SAT})$represents the 0-D ice mass density, Mww = 18.0 *g/mol* is the molecular weight of H_2O, and R = 8.314 *J/mol/K*.

3. Start and End of the PMC Season

[12] The causes for the start and end of the PMC season is one of the main issues of PMC science that needs to be addressed and in particular it is of great importance in serving as an indicator of mesospheric climate change. This topic was implicitly embedded in the AIM prelaunch microphysics objective [*Russell et al.*, 2009], and with a continuous time series of many key variables provided by SOFIE throughout the summer and especially with SOFIE's ability to detect weak clouds, new light can be shed on this problem. Since the start and end of the PMC season addresses the cloud existence rather than its brightness, we use the PMC "appearance" frequency to attack this problem.

3.1. Rapid Onset and Termination of the PMC Season Observed by SOFIE

[13] Figure 2a shows the daily SOFIE PMC frequencies in the 2007–2010 northern seasons. The cloud frequency here refers to the percentage of PMCs detected within the daily measured 15 events. A striking feature in Figure 2a is that for all 4 years there are three fairly distinct stages for the PMC season, starting period, main period, and ending period. At the two ends the cloud frequency rises to nearly 100% or drops to nearly zero within ~10 days. It should be noted however that in 2007 the start of the season was not entirely revealed because reliable SOFIE data collection did not begin until after the season started. Nevertheless, the rapid increase of the cloud frequency is partly captured. For all 4 years, after the solstice and toward the end of the season, the cloud frequency is notably declined from 100%, although the speed of the decline shows interannual variability unlike the variation at the start of the season which is similar for all 4 years. The rapid onset and termination of the PMC appearance was reported as early as 1972 by *Donahue et al.* [1972] but only in the latitude range north of 80°N. Sudden onset and termination of the PMC appearance at high polar latitudes was also discussed by *Thomas* [1984] and *Lübken et al.* [1996],

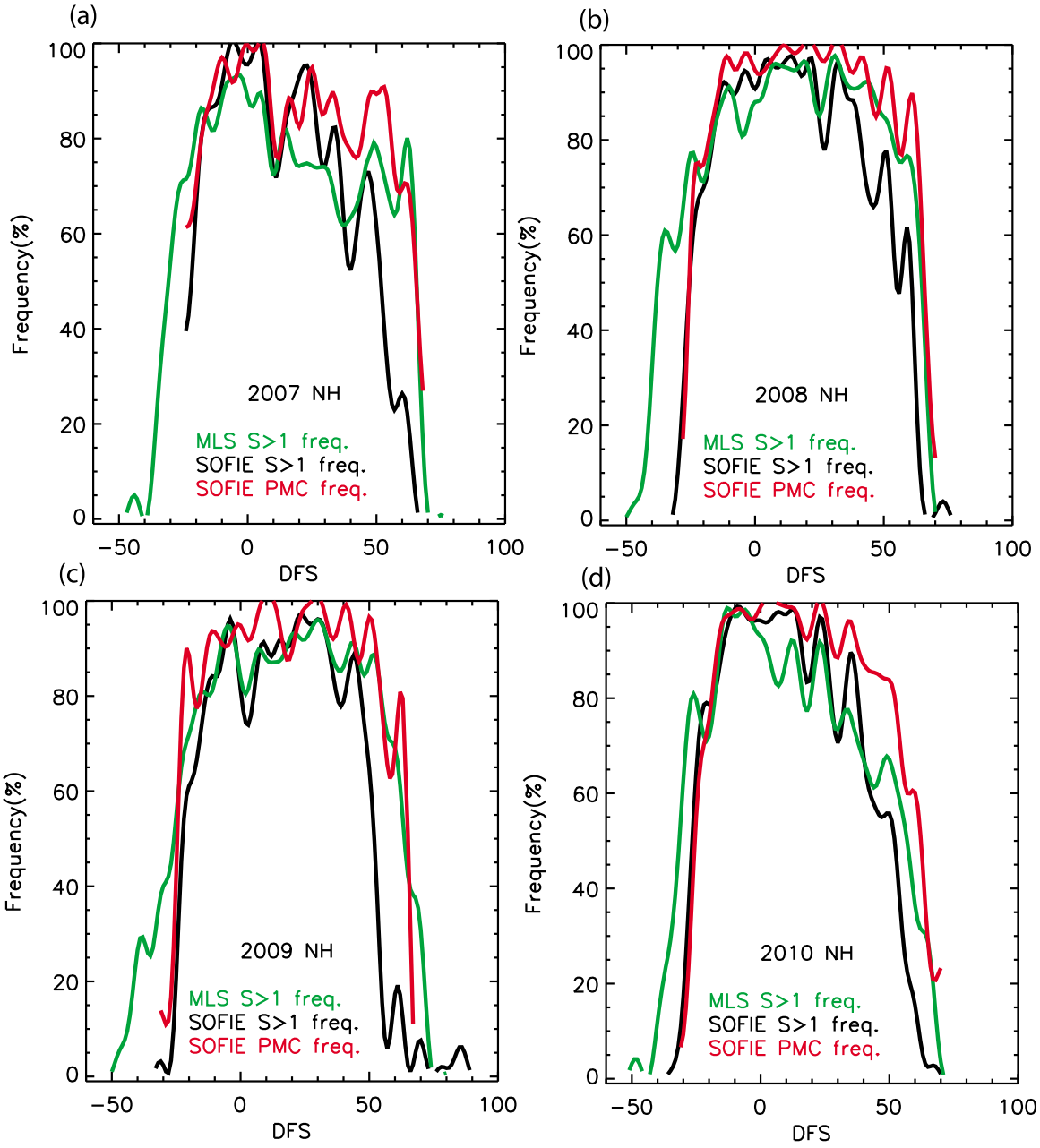

Figure 3. The 0-D frequencies for SOFIE and MLS and the SOFIE PMC frequency. MLS data points are chosen daily within a 2.0° range that is centered at SOFIE latitudes. A 4-day smoothing is applied to each time series.

but never before SOFIE was this occurrence found at such low polar latitudes as 65–75°N. For most PMC data sets retrieved from satellite measurements, the cloud frequency north of 60°N exhibits a rather gradual start and end of the season [*Bailey et al.*, 2005; *DeLand et al.*, 2006; *Petelina et al.*, 2007; *Robert et al.*, 2009]. This is because when the instrument is not sensitive enough to the weak clouds, the brightness threshold has to be set higher, and in such cases the cloud strength (i.e., brightness or albedo) is involved in determining the cloud existence. This can be clarified by examining the SOFIE frequency intraseasonal variation using larger threshold values, shown in Figure 2b. The SOFIE default threshold is approximately ~0.15 ng/m^3 in terms of ice mass density. As the threshold is increased, the overall frequency is reduced, the seasonal start and end become more gradual, and the frequency variation increasingly resembles the ice mass density variation. This last point can be clarified by comparing Figure 2b and Figure 8 in section 4.1 that discusses the ice mass density intraseasonal variations. Figure 2b clearly indicates that the detection of weak clouds can substantially affect the results.

[14] We next examine the 0-D modeled PMC frequency. For a given pair of SOFIE or MLS temperature and H_2O profiles, as long as $S > 1$ is met for any altitude range, mostly around the coldest point, we claim the existence of a cloud. Figure 3 shows the 0-D modeled and the SOFIE observed

PMC frequencies. There are two 0-D modeled frequencies; one using SOFIE v1.022 data and the other using MLS v2.2 data. MLS data is chosen daily at the SOFIE latitude $\pm 1.0°$ range. Excellent qualitative agreement exists between the 0-D modeled and the observed frequencies, i.e., both show rapid onset and termination, and the shorter time scale variations during the main period also agree well. This suggests that the criterion $S > 1$ is a sufficient condition to reproduce the main characteristics of observed PMC frequency intraseasonal variation. In a quantitative sense, the SOFIE 0-D cloud frequency marks a slightly earlier ending period than the observation but a similar starting period. The MLS 0-D cloud frequency on the other hand marks a significantly earlier starting period than the observation but a similar ending period. This finding is consistent for all years of analyses. Since the 0-D cloud frequency depends on both P_{SAT} and P_{H2O}, the difference in either could have caused the discrepancies. We however can quickly rule out the P_{H2O} for two reasons. First, a validation study has verified overall good agreement between MLS and SOFIE water vapor in the NH mesosphere [*Rong et al.*, 2010]. Second, we will later find that the start or end of the PMC season is not sensitive to a small change in the water vapor partial pressure. It is highly probable that the temperature difference between the two data sets is causing these differences. The more extended cloud season shown in the MLS 0-D frequencies suggests that the mesopause temperature in MLS is systematically lower than in SOFIE. But a striking issue here is not the overall temperature bias, but the fact that the start and end appear asymmetric when compared to the observed PMC frequency. If both SOFIE PMC measurements and the 0-D assumption are valid, it points to a conclusion that SOFIE is biased warm at the end while MLS is biased cold at the start. This, however, may not be the only interpretation. For example, *Petelina and Zasetsky* [2009] (also see *Hervig and Gordley* [2010]) argued that when ice is present, the solid-phase temperature, i.e., ice temperature, is more appropriate to describe the thermal state of the PMC region. There is a possibility that toward the end of the season, gas-phase temperature alone is not sufficient to fully describe the thermal state of the cloud region. Although ice temperature cannot be used to predict the start and end of PMC season because its retrieval requires the knowledge of ice existence, when exiting the PMC season the thermal state may have been affected by a long history of ice presence, which could have contributed to the discrepancy at the end. Another noteworthy difference between the 0-D modeled and the observed PMC frequencies is that the latter is generally higher than the former, especially after the solstice when the mesosphere temperature begins to rise. The nearly 100% cloud frequency, which is higher than the maximum ice production ($S > 1$) allows, suggests that the clouds are ubiquitous and exist at locations where the temperature is warmer than the frost point. Horizontal transport is one possible cause. After the solstice the PMCs are fully developed and become increasingly stronger, and during this time the clouds cover all longitudes. Under such a prevailing condition, horizontal transport can further spread them over a more extended spatial range in the presence of a fairly strong easterly wind of about ~30–50 m/s at the PMC altitudes. *Baumgarten et al.* [2011] suggested that the ice particles could behave like a passive tracer for up to an hour and travel several hundred kilometers downstream if no wave structures are involved. Numerical modeling studies are required to test this hypothesis and to pursue other possible causes.

3.2. Latitude Dependence of the 0-D Frequency

[15] We have so far examined the cloud frequencies at SOFIE latitudes using both SOFIE and MLS data and compared the timings of rapid increase and decrease at the start and end of the PMC season. One must then wonder how the SOFIE measurement latitude change affects these timings and the 0-D frequency variations in general.

[16] Figure 4 shows the MLS 0-D frequency in different latitude bands (65–70°N, 70–75°N, 75–80°N, and 80–82°N). For all 4 years, we find that the 0-D modeled start and end days would have been highly consistent between different latitude bands if <5% cloud presence is chosen as a threshold. This is because the condition $S > 1$ is simultaneously met in all latitude bands. We have mentioned above that the temperature latitudinal gradient is smaller at the two ends than in the core of the season, and this is especially true for the daily minimum temperature that is used to claim the first 0-D cloud. We also note that in all latitude bands the maximum frequency can reach ~90–100% although the frequency variation is clearly latitude dependent. In the starting period the 0-D frequencies in all latitude bands are relatively consistent while after the summer solstice toward the end the frequencies on the lower latitudes are more notably declined. Although there is no exact observational evidence to support this latitude dependence of the cloud frequency, it is basically consistent with what Figure 2a shows, that is, there is more variability at the end than at the start of the season. SOFIE PMC frequency did not show severe decline toward the end of the season because the SOFIE latitude reaches 75–80°N after August 15, i.e., ~55 days after the solstice. Direct observational evidence does not currently exist because no data set covering the polar cap region has been obtained with the SOFIE sensitivity.

3.3. Temperature Controls the Onset and Termination of the PMC Season

[17] In Figure 5 we separate the roles of P_{SAT} and P_{H2O} in determining the start and end of the cloud season. Among the 4 years used in our analysis 2010 is shown as an example. The analysis starts by showing all the P_{SAT} and P_{H2O} values from the chosen events. For SOFIE all 15 events per day are included, while for MLS the events are chosen at the SOFIE latitude $\pm$ 1.0° as mentioned above. For each pair of temperature and H_2O profiles the P_{SAT} and P_{H2O} values are taken at the altitude where S maximizes. This altitude is very close to the mesopause in the core of the season. The left-hand vertical axis is logarithmic so that we can see the full ~8–10 order span of P_{SAT} variation from May to September. The blue curves are the daily minimum and median P_{SAT} with a 4-day smoothing applied. The P_{H2O} variation, on the other hand, is nearly flat for the same scale, i.e., before the solstice it exhibits a gradual increase until it reaches a near-constant but slightly increasing level and continues after the solstice. The far more rapid change in P_{SAT} than in P_{H2O} at the start and end of the PMC season supports the argument that temperature is in primary control when entering or exiting the PMC season. Knowing that P_{H2O} is less variable, we simplify its development into a stepwise function, jumping

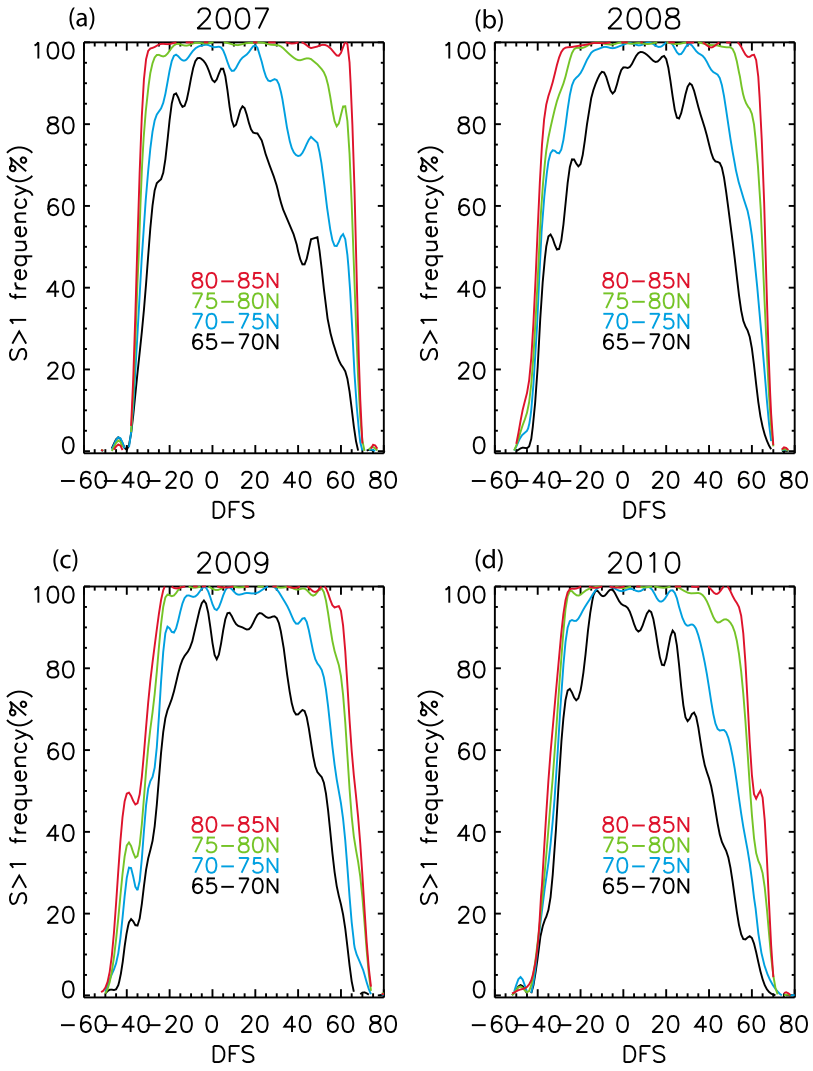

Figure 4. The 0-D frequencies in the different latitudinal bands calculated from MLS temperature and H_2O. A 4-day smoothing is applied to each time series.

from a lower level before the solstice to a higher level after the solstice. Either before or after the solstice, a geometric mean of all the Log(P_{H2O}) values is calculated and a mean P_{H2O} level is obtained accordingly. The two P_{H2O} levels will be used later to obtain a set of 0-D determined start and end days of the cloud season. In the postsolstice stage the P_{H2O} range marked by the dashed lines are determined by the 1-σ standard deviation of all Log(P_{H2O}) values. The dashed lines of SOFIE and MLS P_{H2O} mark a very similar scatter, but it is worth mentioning that the overall MLS P_{H2O} magnitude is about half of SOFIE because the mesopause pressure is lower in MLS. This, however, will not qualitatively affect the result because P_{H2O} does not dominantly control the onset and termination of the cloud season. Through comparing SOFIE and MLS, we note that the intraseasonal variations of SOFIE and MLS P_{SAT} and P_{H2O} are very similar; clearly for both data sets, the coldest day is close to the solstice and the rates of cooling before and the warming after the solstice are very similar. We do, however, note that throughout the PMC season the MLS temperature is on average lower than SOFIE. This temperature difference has been reflected in the 0-D frequencies shown in Figure 3. The daily minima of the two data sets show a large difference, i.e., ~20 K, suggesting that a significant number of MLS measurements indicate a much colder mesopause than what is measured by SOFIE. The daily median difference between the two data sets however is much smaller, being ~10 K or less. The daily maxima of the two data sets are close, and some MLS data points show even warmer temperature than observed by SOFIE. Nevertheless one should note that the daily warmest points, which are mostly above the frost point, are not relevant to PMC formation. Measurements that indicate a colder mesopause than in the SOFIE temperature are not unprecedented before MLS. For example, mesopause temperatures measured by the falling sphere at 69°N can be as low as ~120 K in late July to August [*Lübken et al.*, 1996], pointing to even colder condition than in MLS. The significant discrepancies in the upper mesospheric temperature between falling sphere, MLS, and several other satellite data sets such as ACE, SABER, and SOFIE remain unresolved [e.g., *Schwartz et al.*, 2008]. We have just argued that part of the differences may be attributed to the LT difference. But

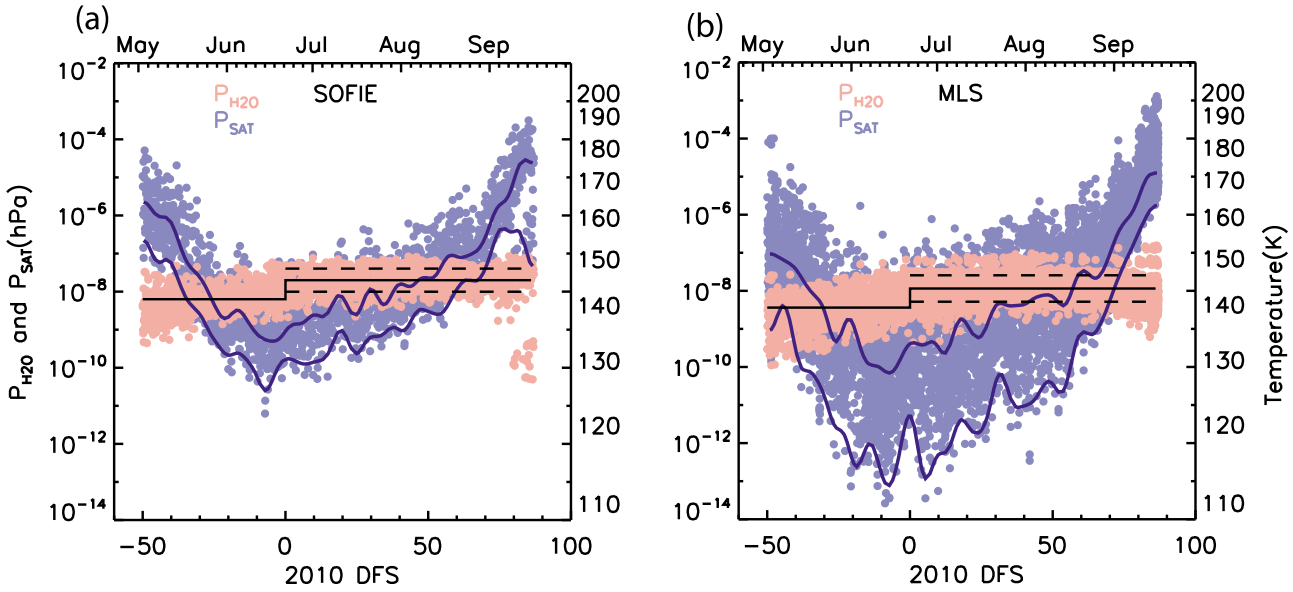

Figure 5. The NH intraseasonal variations of P_{SAT} and P_{H2O} on logarithm scales. The dots are for individual events. For each event the pair of data points is chosen at altitude where S maximizes. The blue curves are daily minimum and median P_{SAT} time series obtained using a 4-day smoothing. The stepwise black lines are mean P_{H2O} before and after summer solstice. The dashed lines (after the solstice) bound the P_{H2O} range that is determined by 1-σ standard deviation of the P_{H2O} values. (a) SOFIE analysis. (b) MLS analysis. The data points are chosen in a 2.0° latitude range that is centered at SOFIE latitudes. Only the analysis for 2010 is shown as an example.

the LT difference cannot account for the full magnitude of the temperature difference. MLS temperature may actually be biased cold. For example, at the start of the PMC season the SOFIE temperature accuracy is better supported by the SOFIE PMC frequency, while the MLS 0-D frequency indicates a start time for which no PMCs were ever reported. We do, however, note that the 0-D assumption is highly simplified and therefore may have limitations. For example, the seasonal onset may appear earlier in the 0-D model than in the real atmosphere owing to the omission of the nucleation. Further research is required to define the extent of these limitations and to better understand the process of ice particle formation in general.

[18] Another noteworthy feature shown in Figure 5a is a bimodal behavior of both P_{SAT} and the corresponding P_{H2O} in September. More specifically, the bimodal behavior refers to the fact that at the end of the summer the data points of P_{SAT} or P_{H2O} are distributed at two levels, respectively. This occurrence is associated with a double-mesopause feature that appears from late August to September in SOFIE temperature. This is a transitional time period when the lower summer mesopause rises to a higher winter mesopause. During this time two temperature local minima, which are about 10–12 km apart, coexist. The double-mesopause does not necessarily result in a bimodal behavior in Figure 5a because the criterion of S being maximized naturally selects the lower one when it is cold enough. In September, however, the lower mesopause warms up considerably and the chosen data point jumps up and down. Although to the best of our knowledge, no in depth study has been conducted so far to clarify the mechanism of the double-mesopause, the presence of a double-layer mesopause was in fact documented in several previous studies such as *von Zahn et al.* [1996] and *States and Gardner* [1999]. In these studies, however, mostly the midlatitude to low-latitude region was the focus of the analyses. As for the cause of the double-mesopause structure, *States and Gardner* [1999] argued that incomplete sampling of the diurnal cycle, for example, nighttime measurements being chosen exclusively, made these disturbances stand out because the double-mesopause occurs preferably during the nighttime. Overall speaking, since the bimodal behavior occurs after the PMC season ends, it is not an immediate concern of this study. But the fact that it appears strikingly clear at the end but not at the start of the summer shares some resemblance to the finding of *Nielsen et al.* [2010], that is, an enhanced 5-day wave activity exists in August but not in May. The MLS temperature does not detect the double mesopause mainly because the MLS vertical resolution is 14–16 km in the summer mesopause altitude region. Furthermore, when a double-mesopause does occur, the upper branch usually exceeds the pressure range of the recommended MLS data usage.

[19] Figure 6 shows the P_{SAT}, P_{H2O}, and cloud frequencies on a linear scale to examine their correlation. The shaded area is between the minimum and twice the median (2× median) P_{SAT}, and the curve in the middle is the median P_{SAT}. Three curves are shown to represent the collective behavior of P_{SAT} for which the supersaturated condition ($S > 1$) is satisfied. Figure 6 indicates that all P_{SAT} curves experience a rapid decrease at the start and a rapid increase at the end of the PMC season, which is just opposite of the behavior of the PMC frequency. This clearly shows that the rapid onset and termination of the PMC season is caused by the P_{SAT} variation. In addition, P_{SAT} variations in the main period, especially those of the median and 2× median P_{SAT} for SOFIE, are roughly anticorrelated with the variations of the PMC

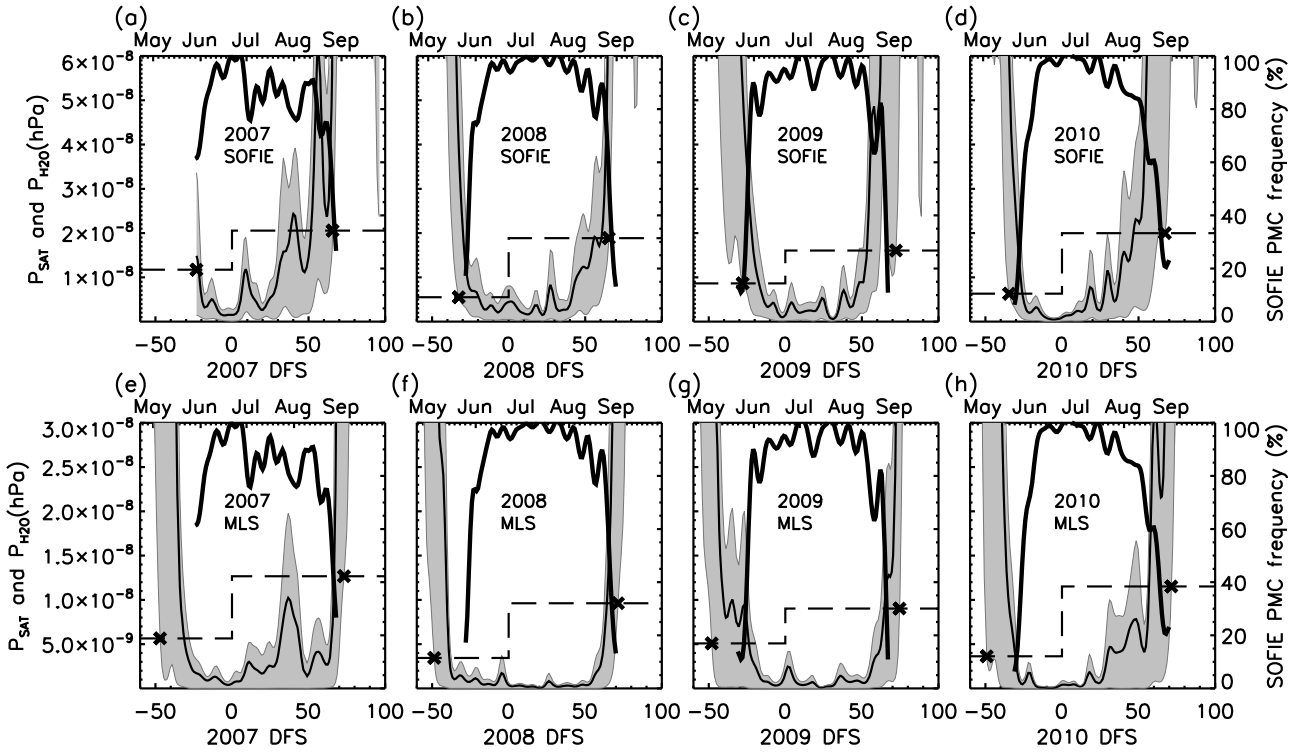

Figure 6. The intraseasonal variations of P_{SAT} and P_{H2O} on linear scales. The shaded area and the thin black line in between are minimum, median, and twice the median of P_{SAT} daily, calculated from (top) SOFIE and (bottom) MLS data. The stepwise lines are the mean P_{H2O} levels shown in Figure 5. The thick black curves are SOFIE observed PMC daily frequencies shown in Figure 3. The cross signs are the closest possible start and end days that are determined by the crossings between the P_{SAT} minimum and the stepwise P_{H2O} lines.

frequency. The anticorrelated relationship holds particularly well for those years that had distinct frequency decline toward the end of the season, i.e., 2007 and 2010. In the MLS analysis, the anticorrelation also holds very well for 2007 and 2010. The decline of the frequency reflects a systematic warming that is substantial enough to make a notable increase in P_{SAT}. On the contrary, if temperature gets increasingly lower and necessarily P_{SAT} becomes indefinitely small, the cloud frequency remains at ~100%. Overall, the analysis above suggests that temperature controls the cloud frequency variation in all stages of the cloud season. This controlling role of temperature on the PMC frequency was also shown by *Fiedler et al.* [2011] who analyzed the diurnal variation of the cloud frequency.

3.4. Start and End Days of the PMC Season

[20] So far we have not discussed the actual days on which the PMCs are first or last detected; instead, we have been more focused on the timings when the cloud frequency substantially increases or decreases. The first and last cloud detection can be affected by a number of factors. For example, low sensitivity to the weak clouds can make the start day appear delayed although SOFIE should not have this problem. Also, an occasional detection of one or two clouds can be due to the fluctuations of temperature or H_2O that favor PMC formation before the systematic onset of the PMC season. In addition, a satellite instrument can only scan a given location at discrete LTs while clouds that occur at other LTs will be missed. All these factors combined can lead to several days of difference in the determined start or end days. For example, in the work of *Bailey et al.* [2005] and *Petelina et al.* [2006] the NH start days are on average between 20 and 25 days before the summer solstice, which are at least 5 days delayed compared to the days shown in this analysis. Owing to these uncertainties, the observed PMC start and end days are not fully robust characteristic. In this study we define a set of 0-D start and end days to compare with the observations. These days are used to describe the timing of a systematic increase or decrease of the 0-D cloud frequency. The combination of the observed and the 0-D start and end days will describe the onset and termination of the PMC season more concretely. The 0-D start and end days are determined by the first and last crossing points (from left to right) between the minimum P_{SAT} and the stepwise P_{H2O} mean levels shown in Figures 5 and 6. The minimum P_{SAT} is used since the 0-D assumption requires only one event meeting the condition of $S > 1$ to form the first cloud.

[21] The SOFIE observed and the 0-D determined PMC start and end days, in terms of days from solstice (DFS), are given in Tables 1a and 1b. We have seen from above that in 2007 the cloud season had already started when SOFIE data

Table 1a. Observed and 0-D Determined Start and End Days

	2007		2008		2009		2010	
	Start	End	Start	End	Start	End	Start	End
SOFIE 0-D	–	65.7	−32.5	65.5	−27.8	72.3	−34.5	67.2
SOFIE Observed	–	68	−28	70	−31	67	−31	70
MLS 0-D	–	73.2	−48.5	71.4	−48.0	74.6	−49.1	71.5

Table 1b. Mean Differences Between the 0-D Determined and Observed Dates Over Different Years and the 1-σ Standard Deviations of These Differences[a]

	Start (Without 2007)	End (All Years)	End (Without 2009)
SOFIE 0-D	-1.6 ± 4.2	-1.1 ± 4.3	-3.2 ± 1.1
MLS 0-D	-18.5 ± 1.8	3.9 ± 3.0	2.7 ± 2.2

[a]The two rows are calculated using either SOFIE 0-D observation or MLS 0-D observation.

became available. So with 2007 being taken out, the 3-year statistics indicate that the SOFIE 0-D start day is on average 1.6 days earlier than the observed start date with a scatter of 4.2 days. The mean difference is smaller than the scatter, roughly indicating that the SOFIE 0-D and observed start days agree well and do not have a significant bias. The MLS 0-D start day, on the other hand, is about 18.5 days earlier than the observation with a scatter of 4.3 days, suggesting a large bias in temperature. The comparisons of the start days reflect what Figure 3 shows on the frequency development at the start. The SOFIE derived end day is on average 1.1 days later than the observed end day with a scatter of 4.3 days, which also supports a good agreement. The reason why we did not see a SOFIE warm bias as suggested in Figure 3 is because in 2009 there is a return of coldness after a substantial warming. If we remove the year 2009, the SOFIE 0-D end day will be 3.2 days earlier than the observation, with a scatter of 1.1 days, which would suggest a warm bias in SOFIE temperature. Similarly, we found that the MLS derived end day is on average 3.9 days later than the observation with a scatter of 3.0 days. If 2009 is excluded, the end day is 2.7 days later than the observation with a scatter of 2.2 days. Both cases indicate that the bias is insignificant. This is roughly consistent with the previous finding (Figure 3) that the MLS 0-D frequency shows strong agreement with the SOFIE PMC frequency during their rapid decrease that marks the termination of the season. As a final point, one should note that although 4 years are far too short to yield any reliable statistics, we do not entirely rely on the statistics in this case. Figure 3 indicates that years 2007–2010 show highly consistent results. The statistics in Tables 1a and 1b mainly tests whether the approach to determine the 0-D start and end days works efficiently and produces results consistent with Figure 3.

[22] Given the approach proposed above to derive the start and end days, one would wonder how the temperature or H_2O change can affect these derived days. A sensitivity study has been performed and the results are summarized as follows. If the temperature is shifted by plus or minus 10 K the start or end date will vary approximately plus or minus 10 days. If the H_2O is changed, it takes about a 10 times wetter or drier mesosphere to make the same difference in the two dates. In practice, a highly concerned issue is whether there is a long-term trend in the cloud seasonal start or end days. The limited number of trend analyses in the past decade or so suggest that neither the H_2O trend (e.g., ~0.05 ppmv/year from 1996 to 2000 in the work of *von Zahn et al.* [2004]) nor the temperature trend (e.g., −0.24 K/decade from 1964 to 1996 in the work of *Lübken* [2000; see also *Beig et al.*, 2003]) in the polar summer mesosphere is large enough to significantly change the start and end of PMC season, especially when the reliability of these trends is still unclear. Nevertheless, assume that the extremely small temperature trend shown by *Lübken* [2000] is present it will take about 4 decades to make the start day 1 day earlier, which is far less than the interannual scale fluctuations. This is consistent with the findings of *Gadsden* [1998a] who suggested that the length of the NH PMC season remains fairly constant over the years.

4. PMC Ice Mass Density

[23] In the following sections we examine how P_{H2O} and P_{SAT} control the ice mass density. Figure 7 shows a scatterplot of 0-D ice mass density values at Z_{max}, denoted by m_{ice}, on the P_{SAT} versus P_{H2O}-P_{SAT} plane. It should be noted that all analyses below are performed at Z_{max}. We use P_{H2O}-P_{SAT} as one dependent variable simply because the 0-D ice mass density is proportional to $(P_{H2O}$-$P_{SAT})/T$. The temperature in the denominator is a negligible factor compared to P_{H2O}-P_{SAT} in controlling the 0-D ice mass density variation. Since P_{H2O} divided by temperature is proportional to the H_2O number density, we take P_{H2O} to be in a very similar role as H_2O number density. The contours reflect all the m_{ice} values using any possible combination of temperature and H_2O while the individual data points are calculated using the SOFIE temperature and H_2O profiles from 2007 to 2010. The same color scheme is applied for both the contours and the dots. It is noted that the contours are parallel to the horizontal axis in most cases, suggesting that m_{ice} does not vary much with P_{SAT}; instead, P_{H2O}-P_{SAT} is in nearly full control of the m_{ice} variation except for the very large m_{ice} (>100 ng/m^3) at which the effect of the temperature becomes notable. But apparently these large values are rarely attained among all SOFIE 0-D modeled m_{ice} values. Another striking feature is that the orientation of the cluster of dots maintains a very

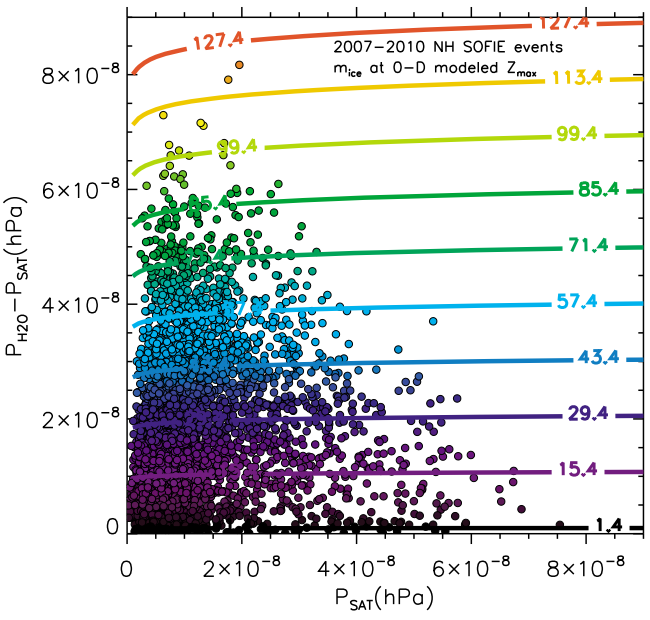

Figure 7. The 0-D ice mass densities on the P_{SAT} versus P_{H2O}-P_{SAT} plane. The dots are ice mass densities calculated using SOFIE temperature and H_2O. The color of any given contour or dot represents the magnitude of ice mass density, in units of ng/m^3.

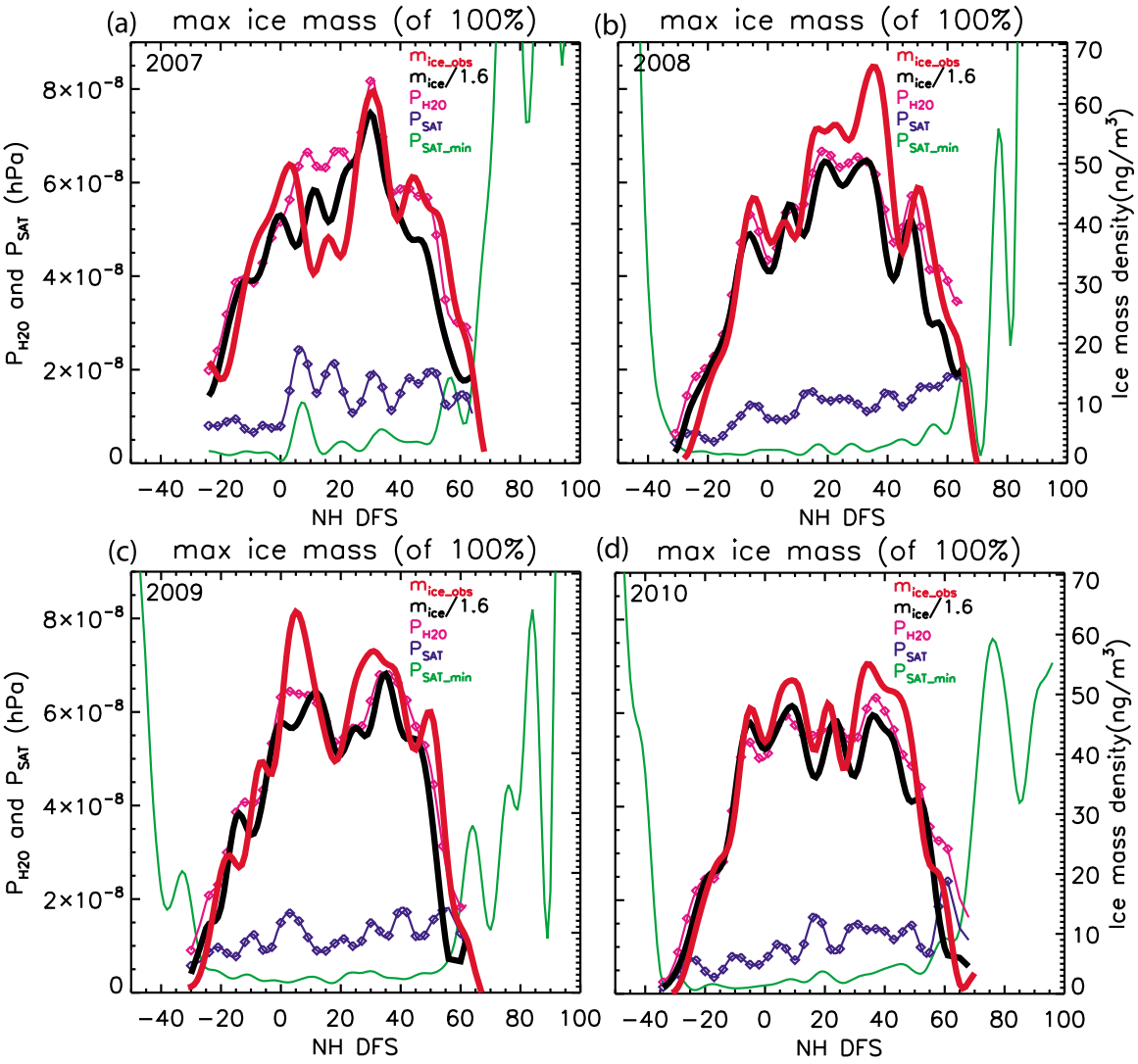

Figure 8. The intraseasonal variations of P_{H2O}, 0-D ice mass density, and SOFIE observed ice mass density for the strong cloud case. Daily values are taken at the cloud peak height. For all the daily values the maximum ice mass density is used and then the corresponding P_{H2O} and P_{SAT} are chosen. The daily minimum P_{SAT} at cloud peak height is also plotted. A 4-day smoothing is applied for all the time series.

small angle to the axis of P_{H2O}-P_{SAT}, indicating that P_{SAT} remains fairly low with respect to P_{H2O}-P_{SAT}. This suggests that as the m_{ice} increases, P_{H2O} experiences a more drastic change than P_{SAT} and therefore P_{H2O} takes a dominant role in the m_{ice} variation.

4.1. Comparison of the 0-D and the SOFIE Observed Ice Mass Densities on Intraseasonal Scales

[24] In this subsection we compare the 0-D modeled and the SOFIE observed ice mass densities on intraseasonal scales and further examine their relationship with P_{SAT} and P_{H2O}. The observed ice mass density at the observed Z_{max} is denoted by m_{ice_obs}. Although Figure 7 suggests that P_{H2O} is in control of m_{ice} variation in an overall sense, more detailed analyses are needed to further separate the roles of P_{H2O} and P_{SAT}. It is also necessary to separate different time scales or cloud strengths since the relative importance of P_{H2O} and P_{SAT} may vary with these factors. In this paper we are particularly interested in studying what controls the m_{ice} variation at different cloud strengths. In order to define the strong and weak cloud cases, we sort the m_{ice} or m_{ice_obs} values daily from smallest to largest. The strong cloud case is defined as the time series using the daily maximum ice mass density values. In defining the weak cloud case, two steps are required. First, the first 20% of the daily sorted events are chosen; second, among the chosen events the maximum value is selected to represent the weak cloud case. We did not simply use the daily minimum ice mass density because the daily weakest cloud is most severely affected by the cloud detection uncertainty. The medium cloud case, which uses 50% threshold instead of 20%, is included in some analyses but is not the focus of the discussion. It should be pointed out here that the above definitions only pertain to their meanings in a relative sense and are only appropriate for the main period of the season during which the daily cloud frequencies are persistently high. While at the seasonal start or end, the clouds are fewer and generally weaker, and therefore all clouds should be considered weak.

Table 2. Correlation Coefficients Between P_{SAT}, P_{H2O}, m_{ice}, and m_{ice_obs} in Strong, Medium, and Weak Cloud Cases and Their Confidence Levels (in the Parentheses)[a]

Correlation Coefficient (Confidence Level %)	2007	2008	2009	2010
	P_{H2O} Versus P_{SAT}			
Strong	0.62 (99.9)	0.56 (99.9)	0.41 (99.9)	0.43 (99.9)
Median	0.88 (99.9)	0.64 (99.9)	0.76 (99.9)	0.70 (99.9)
Weak	0.94 (99.9)	0.78 (99.9)	0.88 (99.9)	0.90 (99.9)
	P_{H2O} Versus m_{ice}			
Strong	0.95 (99.9)	0.97 (99.9)	0.98 (99.9)	0.96 (99.9)
Median	0.84 (99.9)	0.78 (99.9)	0.81 (99.9)	0.89 (99.9)
Weak	0.08 (50.0)	0.69 (99.9)	0.29 (99.0)	0.56 (99.9)
	m_{ice} Versus m_{ice_obs}			
Strong	0.81 (99.9)	0.93 (99.9)	0.88 (99.9)	0.96 (99.9)
Median	0.87 (99.9)	0.86 (99.9)	0.88 (99.9)	0.91 (99.9)
Weak	0.37 (99.9)	0.78 (99.9)	0.71 (99.9)	0.75 (99.9)

[a]Note that the time series of the strong and weak cloud cases are shown in Figures 8 and 9.

[25] Figure 8 shows the intraseasonal time series of m_{ice_obs}, m_{ice}, and the corresponding P_{H2O} and P_{SAT} in the strong cloud case. P_{SAT_min} at Z_{max} is also overplotted. Although P_{SAT_min} is not a key variable in the ice mass density investigation, it is shown here to confirm a rapid start and end of the cloud season (see Figure 5). A 4-day smoothing is applied to each time series to remove any random variability and to highlight the variation on longer intraseasonal scales. In Figure 8 we first note that the m_{ice} divided by a factor of 1.6 follows a very similar intraseasonal variation to the m_{ice_obs}, indicating that the 0-D model reproduces the intraseasonal variation very well. The factor 1.6 is empirically determined based on the analysis of ice mass density at the cloud peak height. The fact that the 0-D model systematically overestimates the ice production is well expected because it omits the nucleation barrier and the ice particle growth [*Hervig et al.*, 2009b; *Hervig and Gordley*, 2010]. The correlation coefficients (see Table 2) between the m_{ice} and m_{ice_obs} reach 0.9 on average, with the lowest and the highest coefficients being 0.81 in 2007 and 0.96 in 2010, respectively. We also note extremely high correlation between m_{ice} and P_{H2O}, with the coefficient varying from 0.95 to 0.98. The corresponding P_{SAT}, on the other hand, shows relatively poor correlation with m_{ice} or P_{H2O}; the P_{SAT} and P_{H2O} correlation coefficient varies between 0.41 and 0.62. Although substantially lower than the other coefficients in the strong cloud case, these coefficients reflect an inherently significant correlation between P_{H2O} and P_{SAT}, i.e., their confidence levels remain at 99.9%. This is because, in some cases, the variations in P_{H2O} and P_{SAT} are primarily caused by the cloud height variation instead of a fundamental change in the environmental temperature or H_2O. In the cloud region below the mesopause, $\log(P_{H2O})$ and $\log(P_{SAT})$ both decrease monotonically with altitude, so the variations of P_{H2O} and P_{SAT} are not entirely independent. The facts that P_{H2O} far exceeds the P_{SAT} in magnitude in the core of the season and that P_{H2O} and m_{ice} are strongly correlated both support a conclusion that P_{H2O} is in dominant control of the m_{ice} variation in the strong cloud case. At this point we can immediately apply this conclusion to what *DeLand et al.* [2007] have found about a long-term upward trend of the SBUV cloud albedo. Since SBUV instruments detected only bright clouds, we assume that the SBUV measured PMCs match the strong cloud case. Accordingly, we expect a similar upward trend in the mesospheric H_2O over the last 30 years.

[26] Figure 9 shows the weak cloud case. Similar to the strong cloud case, we see fairly good agreement between the $m_{ice}/1.6$ and the m_{ice_obs} in magnitude as well as the overall seasonal variation. The correlation coefficient of the m_{ice} and m_{ice_obs} varies from 0.72 to 0.79 in 2008–2010, but in 2007 it only reaches 0.39. In the 2007 case we see fairly good agreement in the magnitude, and yet a low correlation coefficient is obtained because during the two short periods centered at DFS 15 and after DFS 60 there are anticorrelations that would reduce the correlation coefficient. However, even with the 2007 taken out, the overall correlation between m_{ice} and m_{ice_obs} is still lower than in the strong cloud case. This is mostly caused by a larger uncertainty induced in the weak cloud case, i.e., as P_{H2O} and P_{SAT} are comparable in magnitude and the uncertainties in both variables can contribute greatly to the P_{H2O}-P_{SAT}. A clearly notable characteristic in the weak cloud case is that the P_{H2O} and P_{SAT} roughly vary in concert on intraseasonal scales. As a result the correlation coefficient between the P_{H2O} and P_{SAT} reaches ~0.88 on average. This is very different from the strong cloud case that shows a substantially poorer correlation between P_{H2O} and P_{SAT}. Another difference from the strong cloud case is that the correlation coefficient between the P_{H2O} and m_{ice} is highly variable, varying drastically from 0.08 in 2007 to 0.69 in 2008. This should be expected since we have known from the above that neither P_{H2O} nor P_{SAT} alone dominantly controls the m_{ice} variation. Rather, their roles are basically equal and a given change in either can have a significant effect on m_{ice}. Figure 10 shows the same set of plots as Figures 8 and 9 except that daily averages of all clouds are shown. Examining the daily average is a necessary step because one would wonder whether it is a strong or weak cloud case in average sense. By viewing Figure 10, we can argue conclusively that the daily average of all clouds behaves more like the strong cloud case.

4.2. Relative Importance of the P_{H2O} and P_{SAT} in Controlling the Ice Mass Density

[27] Although the 0-D model has no sensitivity to time, it has proven to be highly effective in reproducing the intraseasonal variation of the observed ice mass density in both strong and weak cloud cases. These results suggest that the 0-D model should also accurately represent longer time scale variations such as those reported by *DeLand et al.* [2007] that are based on seasonal averages. As a further step, it is worthwhile to quantify the relative importance of P_{H2O} and P_{SAT} to the 0-D ice mass density in a general sense. A scatterplot of 0-D ice mass density on the plane of $\log(P_{SAT})$ versus $\log(P_{H2O})$ is shown in Figure 11. The daily P_{SAT} and P_{H2O} values are taken from Figures 8 and 9, representing the strong and weak cloud cases, respectively. The data points in between (the green dots) represent the medium cloud case. The logarithm scale is used to reveal the temperature dependence. Figure 11 suggests that as the environment gets colder and wetter, and necessarily m_{ice} gets larger, i.e., toward the right-lower corner, the m_{ice} contours become increasingly parallel to the axis of $\log(P_{SAT})$, suggesting that

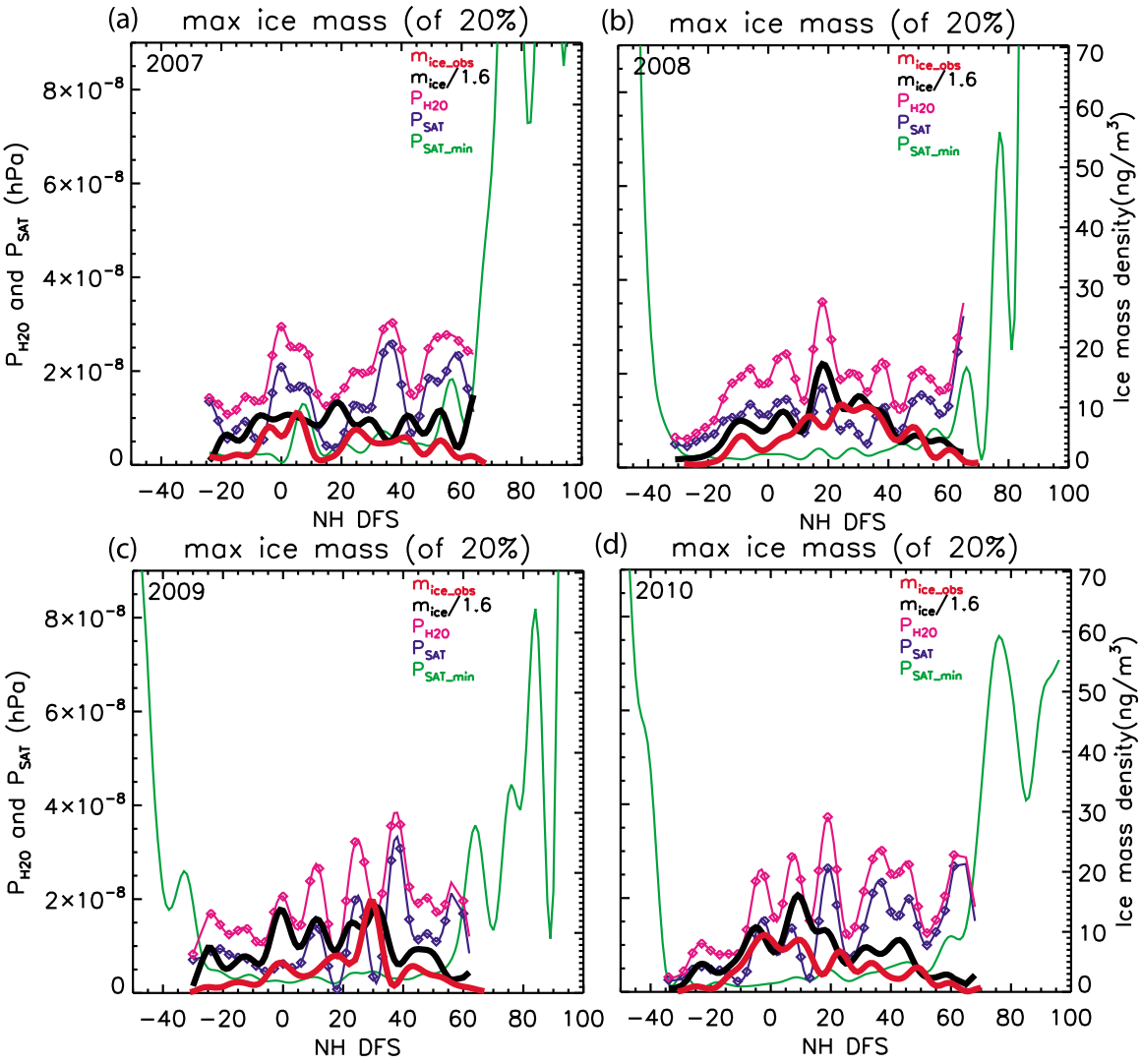

Figure 9. Same as Figure 8 except for the weak cloud case. The definition of the weak cloud case is given in section 4.1.

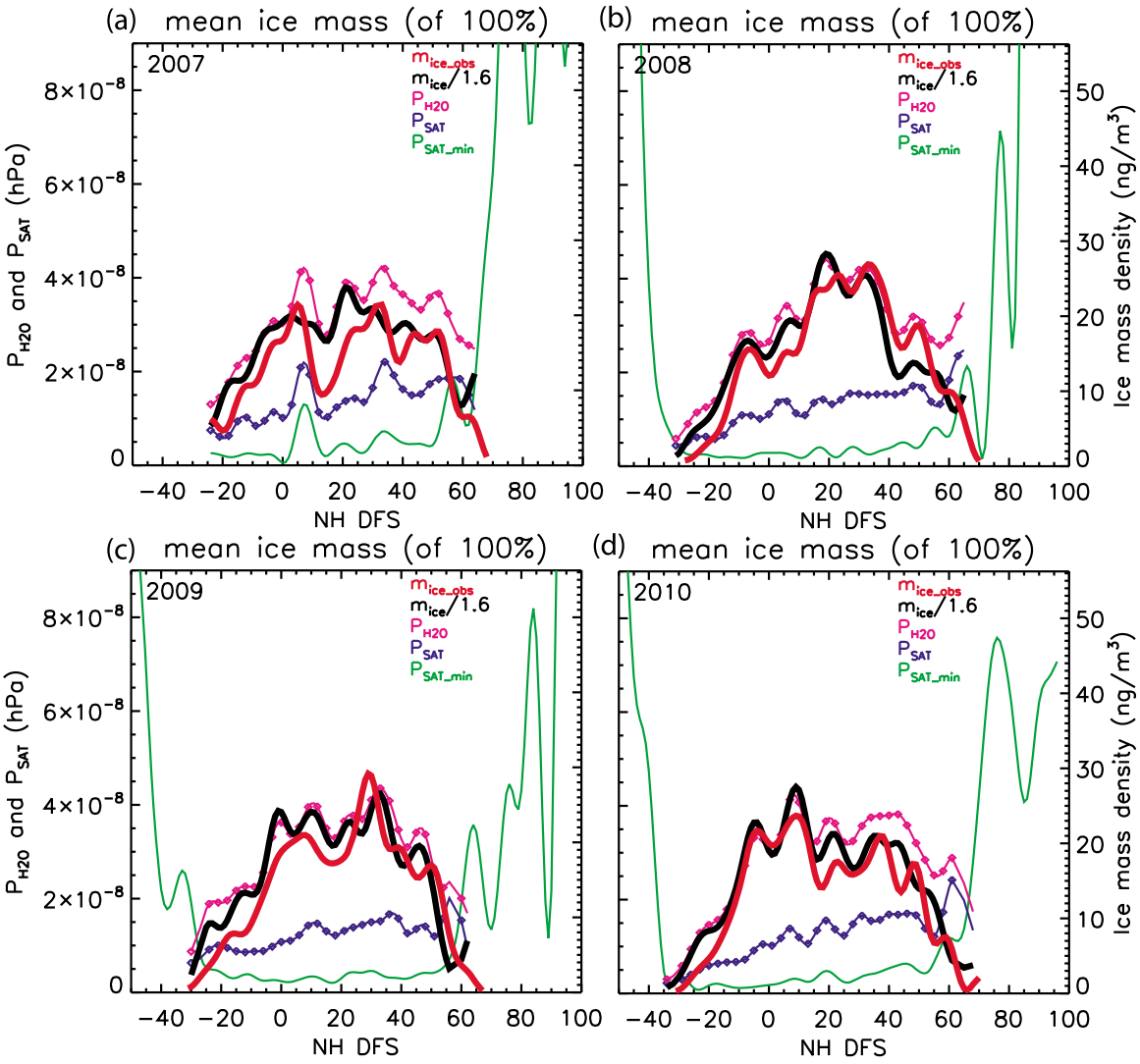

Figure 10. Same as Figure 8 except that the ice mass density is the daily mean of all the calculated or observed clouds. This represents the daily averaged case.

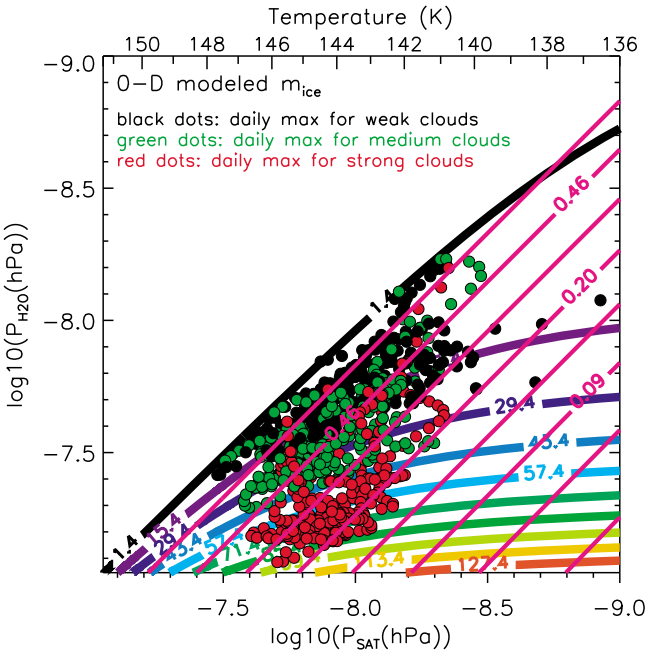

Figure 11. The rainbow-colored contours represent all 0-D ice mass density values on the log10(P_{H2O}) versus log10 (P_{SAT}) plane. Along each pink line the slopes of the contours remain constant. On the basis of the equal-spacing of logarithm, the contour values are chosen as 0.04, 0.06, 0.09, 0.14, 0.20, 0.30, 0.46, and 0.68, respectively. The three sets of dots with different colors are daily P_{H2O} and P_{SAT} pairs for strong (red), median (green), and weak cloud (black) cases in the SOFIE related calculations. Note that the strong and weak cloud cases are shown in Figures 8 and 9.

the m_{ice} variation occurs increasingly predominantly along the log(P_{H2O}) axis. In other words, at the lower right corner of Figure 11 P_{H2O} is in nearly full control of the m_{ice} variation. In reality however m_{ice} may not actually reach the large values in the lower right corner given geophysically reasonable temperature and H_2O, such as those m_{ice} values calculated from the SOFIE temperature and H_2O. To actually quantify the relative importance between P_{H2O} and P_{SAT}, we calculate the m_{ice} contour slopes, shown by the pink lines. Along each pink line the relative importance of P_{H2O} and P_{SAT} is considered constant, and the importance level of P_{H2O} rises as the slope reduces. Observing the three sets of data points, we note that as the clouds get stronger, the clusters move toward lower slope values, suggesting that the P_{H2O} becomes increasingly more in control. For example, the cluster of dots for the strong cloud case is riding on the 0.2 line, suggesting that P_{H2O} is approximately 5 times more important than P_{SAT} in controlling the m_{ice} variation. It is also noted that the dots are less clustered and more oriented in the weaker cloud cases. For example, in the weak cloud case the dots spread along the diagonal line, i.e., $P_{SAT} = P_{H2O}$ line, which explains the correlated changes of the two variables shown in Figure 9; the m_{ice} values can spread more extensively because weaker clouds can form for a much broader range of P_{H2O}, i.e., drier and colder conditions combined, unlike the stronger clouds that can only form under higher P_{H2O}, or wetter condition, regardless of P_{SAT}.

4.3. Implications for Long-Term PMC Trends

[28] What Figure 11 shows may hold for PMC variations on many different time or spatial scales, and further research is needed to explore these possibilities. But the most important issue for the scientific community at present is the long-term PMC trend. If such a trend does exist as suggested by recent papers, it is essential to find out whether it is H_2O or temperature that is driving it. Studies using cloud observations taken during the core of PMC season [e.g., *Romejko et al.*, 2003; *DeLand et al.*, 2007] have indicated that there has been a multidecadal upward trend in the PMC (or NLC) brightness in the last 30–40 years. Results presented earlier in this paper suggest that the reason for these long-term PMC increases are due to H_2O changes and therefore corresponding H_2O observations should show consistent trends. However, there is not yet any conclusive finding regarding long-term H_2O changes since no reliable long-term H_2O records currently exist for the PMC region during summer. However, as mentioned above, an upward H_2O trend was found in the period 1996–2000 at ~80 km altitude at the Alomar observatory (69°N) in polar summer [*von Zahn et al.*, 2004]. It was argued cautiously by these authors that inclusion of such a trend in a NLC model results in an upward trend in the cloud albedo that roughly agrees with the SBUV observations. Nevertheless, a 5-year record is far too short to support a definitive long-term trend owing to the intervention of a series of shorter or longer time scale variations, among which the most prominent is the solar cycle effect. A Halogen Occultation Experiment instrument on UARS satellite (HALOE) [*Russell et al.*, 1993] H_2O analysis performed by *Hervig and Siskind* [2006] has shown a clear solar cycle effect but no significant trend in the polar summer mesosphere. However, HALOE latitude coverage in summer is poor and varies with year, and therefore the result may change when different sampling approaches are used. Overall, more reliable and longer time series are required to verify the consistency between the PMC brightness and H_2O variations.

5. Summary and Conclusions

[29] The rapid onset and termination of the PMC season, and the intraseasonal variation of the ice mass density, were investigated using both the SOFIE data set [*Gordley et al.*, 2009; *Hervig et al.*, 2009a] and a 0-D model [*Hervig et al.*, 2009b]. The SOFIE PMC data set provides unprecedented observational support for the 0-D modeled cloud frequency and ice mass density so that the respective roles taken by temperature and H_2O can be evaluated. The 0-D model assumes ice being produced whenever the supersaturation ratio (S) is greater than one. In such an optimal condition, the ice production is only dependent on temperature and H_2O, i.e., in the form of P_{SAT} and P_{H2O} in this paper. The 0-D assumption was never used as a primary framework to interpret PMC changes in studies of the last few decades because a number of factors that are ignored in the 0-D assumption, such as nucleation, transport of cloud particles via the atmospheric flow field, and ice particle fall velocity, were considered critically important in affecting the PMC variation. The 0-D assumption was brought to light after the SOFIE data analyses indicated that P_{SAT} and P_{H2O} take on controlling roles in the PMC frequency and ice mass density

variations. The SOFIE data set provides a natural platform to study the relationship between PMCs, P_{SAT}, and P_{H2O} because the related variables are simultaneously measured and also because better temporal and spatial details are resolved in SOFIE than in other satellite data sets.

[30] The intraseasonal variation of the SOFIE observed PMC frequency indicates a rapid onset and termination of the PMC season. During the main period of the season the frequency remains at ~80–100%. The SOFIE and MLS 0-D modeled frequencies also indicate a rapid seasonal onset and termination, showing excellent qualitative agreement with the SOFIE observed PMC frequency. Furthermore, the SOFIE 0-D frequency indicates a starting period that agrees well with the observations but an ending period that is a few days earlier. The MLS 0-D frequency indicates an ending period that agrees well with the observations but a starting period that is ~15–20 days earlier. It was argued that such discrepancies between the 0-D and the SOFIE observed PMC frequencies could have been caused by a temperature bias between SOFIE and MLS data. We conclude that it is the temperature variation rather than H_2O variation that dominantly controls the PMC seasonal onset and termination. When interpreting the asymmetry between the 0-D determined start and end in relative to the PMC observation, we argue that on exiting the cloud season, owing to a long history of ice existence, gas-phase temperature alone may appear warmer than desired in determining the end of the season; rather, ice-temperature should also be considered. These assertions, while logical, remain unproven and unresolved.

[31] Throughout the summer, P_{SAT} experiences over 8 orders of magnitude variation, whereas the P_{H2O} variation is nearly flat in comparison. The much smaller variation of P_{H2O} is represented by a stepwise function using two P_{H2O} levels, one averaged before and the other after the solstice, respectively. The collective behavior of all P_{SAT} values that meet the condition $S > 1$ shows a rapid decrease at the start and rapid increase at the end of the season, which is exactly opposite to the variation of the cloud frequency. P_{SAT} and the cloud frequency are also anticorrelated in detailed intraseasonal variations. This suggests that P_{SAT}, or temperature variation, controls the cloud frequency variation throughout the cloud season. The estimated start (or end) day is defined as the day on which the daily minimum P_{SAT} goes below (or above) the presolstice (or postsolstice) level of the P_{H2O}. The 0-D determined start and end days are in good agreement with what the observed cloud frequencies suggest regarding the timing of the onset and termination of the cloud season.

[32] SOFIE observed and 0-D modeled ice mass densities, i.e., m_{ice_obs} and m_{ice}, are highly correlated on intraseasonal scales, with the correlation coefficient being ~0.9 and ~0.7 in the strong and weak cloud cases, respectively. As a further step it is important to clarify how P_{H2O} and P_{SAT} control m_{ice}. P_{H2O} is in dominant control of the m_{ice} variation in the strong cloud case, while in the weak cloud case P_{H2O} and P_{SAT} vary in concert and both have similar and significant effects on the m_{ice} variation. On the basis of the SOFIE 0-D model results we conclude that the P_{H2O} is about 5 times more important than P_{SAT} in the strong cloud case. However, this factor may very well change if the mesospheric temperature is systematically warmer or colder than observed by SOFIE and it will not be definitive before a better consensus about the mesospheric temperature is reached. Finally, we point out that for both the observed and modeled PMCs, the daily average in the core of the season resembles a strong cloud case. As a result, we conclude that the long-term upward trend of cloud brightness reported by *DeLand et al.* [2007] should be accompanied by an upward trend of H_2O.

[33] **Acknowledgment.** Funding of the AIM mission was provided by NASA's Small Explorers Program under the contract NAS5–03132. Many thanks are given to the SOFIE/AIM and other AIM team members for constant support, encouragement, and valuable advice for improvement on this work. We thank the SOFIE retrieval team for providing the SOFIE PMC data set and SOFIE level2 data set. We also thank the MLS/Aura retrieval team for making the MLS level2 data available online.

References

Bailey, S. M., A. W. Merkel, G. E. Thomas, and J. N. Carstens (2005), Observations of polar mesospheric clouds by the Student Nitric Oxide Explorer, *J. Geophys. Res.*, *110*, D13203, doi:10.1029/2004JD005422.

Baumgarten, G., A. Chandran, J. Fiedler, P. Hoffmann, N. Kaifler, J. D. Lumpe, A. W. Merkel, C. E. Randall, D. W. Rusch, and G. E. Thomas (2011), On the horizontal and temporal structure of noctilucent clouds as observed by satellite and lidar at ALOMAR (69N), *Geophys. Res. Lett.*, *39*, L01803, doi:10.1029/2011GL049935.

Beig, G., et al. (2003), Review of mesospheric temperature trends, *Rev. Geophys.*, *41*(4), 1015, doi:10.1029/2002RG000121.

Bernath, P. F., et al. (2005), Atmospheric Chemistry Experiment (ACE): Mission overview, *Geophys. Res. Lett.*, *32*, L15S01, doi:10.1029/2005GL022386.

DeLand, M. T., E. P. Shettle, G. E. Thomas, and J. J. Olivero (2006), A quarter-century of satellite polar mesospheric cloud observations, *J. Atmos. Sol. Terr. Phys.*, *68*, 9–29, doi:10.1016/j.jastp.2005.08.003.

DeLand, M. T., E. P. Shettle, G. E. Thomas, and J. J. Olivero (2007), Latitude-dependent long-term variations in polar mesospheric clouds from SBUV version 3 PMC data, *J. Geophys. Res.*, *112*, D10315, doi:10.1029/2006JD007857.

Donahue, T. M., B. Guenther, and J. E. Blamont (1972), Noctilucent clouds in daytime: Circumpolar particulate layers near the summer mesopause, *J. Atmos. Sci.*, *29*, 1205–1209, doi:10.1175/1520-0469(1972)029<1205:NCIDCP>2.0.CO;2.

Fiedler, J., G. Baumgarten, U. Berger, P. Hoffmann, N. Kaifler, and F.-J. Lübken (2011), NLC and the background atmosphere above ALOMAR, *Atmos. Chem. Phys.*, *11*, 5701–5717, doi:10.5194/acp-11-5701-2011.

Gadsden, M. (1998a), The north-west Europe data on noctilucent clouds: A survey, *J. Atmos. Sol. Terr. Phys.*, *60*, 1163–1174, doi:10.1016/S1364-6826(98)00072-8.

Gadsden, M. (1998b), Noctilucent clouds seen at 60°N: Origin and development, *J. Atmos. Sol. Terr. Phys.*, *60*, 1763–1772, doi:10.1016/S1364-6826(98)00154-0.

Garcia, R. R., and S. Solomon (1985), The effect of breaking gravity waves on the dynamics and chemical composition of the mesosphere and lower thermosphere, *J. Geophys. Res.*, *90*, 3850–3868, doi:10.1029/JD090iD02p03850.

Gordley, L. L., et al. (2009), The solar occultation for ice experiment, *J. Atmos. Sol. Terr. Phys.*, *71*, 300–315, doi:10.1016/j.jastp.2008.07.012.

Gumbel, J., and B. Karlsson (2011), Intra- and inter-hemispheric coupling effects on the polar summer mesosphere, *Geophys. Res. Lett.*, *38*, L14804, doi:10.1029/2011GL047968.

Hervig, M. E., and L. L. Gordley (2010), Temperature, shape, and phase of mesospheric ice from Solar Occultation for Ice Experiment observations, *J. Geophys. Res.*, *115*, D15208, doi:10.1029/2010JD013918.

Hervig, M., and D. Siskind (2006), Decadal and inter-hemispheric variability in polar mesospheric clouds, water vapor, and temperature, *J. Atmos. Sol. Terr. Phys.*, *68*, 30–41, doi:10.1016/j.jastp.2005.08.010.

Hervig, M. E., L. L. Gordley, J. M. Russell III, S. Bailey, and G. Baumgarten (2009a), Interpretation of SOFIE PMC measurements: Cloud identification and derivation of mass density, particle shape, and particle size, *J. Atmos. Sol. Terr. Phys.*, *71*, 316–330, doi:10.1016/j.jastp.2008.07.009.

Hervig, M. E., M. H. Stevens, L. L. Gordley, L. E. Deaver, J. M. Russell III, and S. M. Bailey (2009b), Relationships between PMCs, temperature and water vapor from SOFIE observations, *J. Geophys. Res.*, *114*, D20203, doi:10.1029/2009JD012302.

Jensen, E., and G. E. Thomas (1988), A growth-sedimentation model of polar mesospheric clouds' comparison with SME measurements, *J. Geophys. Res.*, *93*(D3), 2461–2473, doi:10.1029/JD093iD03p02461.

Kirkwood, S., and K. Stebel (2003), Influence of planetary waves on noctilucent cloud occurrence over NW Europe, *J. Geophys. Res.*, *108*(D8), 8440, doi:10.1029/2002JD002356.

Lambert, A., et al. (2007), Validation of the Aura Microwave Limb Sounder middle atmosphere water vapor and nitrous oxide measurements, *J. Geophys. Res.*, *112*, D24S36, doi:10.1029/2007JD008724.

Lübken, F.-J. (2000), Nearly zero temperature trend in the polar summer mesosphere, *Geophys. Res. Lett.*, *27*, 3603–3606, doi:10.1029/2000GL011893.

Lübken, F.-J., K.-H. Fricke, and M. Langer (1996), Noctilucent clouds and the thermal structure near the Arctic mesopause in summer, *J. Geophys. Res.*, *101*(D5), 9489–9508, doi:10.1029/96JD00444.

Lübken, F.-J., M. Rapp, and I. Strelnikova (2007), The sensitivity of mesospheric ice layers to atmospheric background temperatures and water vapor, *Adv. Space Res.*, *40*, 794–801, doi:10.1016/j.asr.2007.01.014.

Murphy, D. M., and T. Koop (2005), Review of the vapour pressure of ice and super-cooled water for atmospheric applications, *Q. J. R. Meteorol. Soc.*, *131*, 1539–1565, doi:10.1256/qj.04.94.

Nielsen, K., D. E. Siskind, S. D. Eckermann, K. W. Hoppel, L. Coy, J. P. McCormack, S. Benze, C. E. Randall, and M. E. Hervig (2010), Seasonal variation of the quasi 5-day planetary wave: Causes and consequences for polar mesospheric cloud variability in 2007, *J. Geophys. Res.*, *115*, D18111, doi:10.1029/2009JD012676.

Petelina, S. V., and A. Y. Zasetsky (2009), Temperature of mesospheric ice retrieved from the O-H stretch band, *Geophys. Res. Lett.*, *36*, L15804, doi:10.1029/2009GL038488.

Petelina, S., E. J. Llewellyn, D. A. Degenstein, and N. D. Lloyd (2006), Odin/OSIRIS limb observations of polar mesospheric clouds in 2001–2003, *J. Atmos. Sol. Terr. Phys.*, *68*, 42–55, doi:10.1016/j.jastp.2005.08.004.

Petelina, S., E. J. Llewellyn, and D. A. Degenstein (2007), Properties of polar mesospheric clouds measured by ODIN/OSIRIS in the northern hemisphere in 2002–2005, *Can. J. Phys.*, *85*, 1143–1158, doi:10.1139/P07-092.

Rapp, M., and G. E. Thomas (2006), Modeling the microphysics of mesospheric ice particles: Assessment of current capabilities and basic sensitivities, *J. Atmos. Sol. Terr. Phys.*, *68*, 715–744, doi:10.1016/j.jastp.2005.10.015.

Remsberg, E. E., et al. (2008), Assessment of the quality of the Version 1.07 temperature versus pressure profiles of the middle atmosphere from TIMED/SABER, *J. Geophys. Res.*, *113*, D17101, doi:10.1029/2008JD010013.

Robert, C. E., C. Savigny, J. P. Burrows, and G. Baumgarten (2009), Climatology of noctilucent cloud radii and occurrence frequency using SCIAMACHY, *J. Atmos. Sol. Terr. Phys.*, *71*, 408–423.

Romejko, V. A., P. A. Dalin, and N. N. Pertsev (2003), Forty years of noctilucent cloud observations near Moscow: Database and simple statistics, *J. Geophys. Res.*, *108*(D8), 8443, doi:10.1029/2002JD002364.

Rong, P., J. M. Russell III, L. Gordley, M. Hervig, L. Deaver, D. Siskind, P. Bernath, and K. A. Walker (2010), Validation of v1.022 mesospheric water vapor observed by the SOFIE instrument onboard the AIM satellite, *J. Geophys. Res.*, *115*, D24314, doi:10.1029/2010JD014269.

Russell, J. M., III, L. L. Gordley, J. H. Park, S. R. Drayson, D. H. Hesketh, R. J. Cicerone, A. F. Tuck, J. E. Frederick, J. E. Harries, and P. Crutzen (1993), The halogen occultation experiment, *J. Geophys. Res.*, *98*(D6), 10,777–10,797, doi:10.1029/93JD00799.

Russell, J. M., III, M. G. Mlynczak, L. L. Gordley, J. J. L. Tansock, and R. Esplin (1999), Overview of the SABER experiment and preliminary calibration results, in *Optical Spectroscopic Techniques and Instrumentation for Atmospheric and Space Research III*, edited by A. M. Larar, *Proc. SPIE*, *3756*, 277–288.

Russell, J. M., III, et al. (2009), The Aeronomy of Ice in the Mesosphere (AIM) mission: Overview and early science results, *J. Atmos. Sol. Terr. Phys.*, *71*, 289–299, doi:10.1016/j.jastp.2008.08.011.

Russell, J. M., III, P. Rong, S. M. Bailey, M. E. Hervig, and S. V. Petelina (2010), Relationship between the summer mesopause and polar mesospheric cloud heights, *J. Geophys. Res.*, *115*, D16209, doi:10.1029/2010JD013852.

Schwartz, M. J., et al. (2008), Validation of the Aura Microwave Limb Sounder temperature and geopotential height measurements, *J. Geophys. Res.*, *113*, D15S11, doi:10.1029/2007JD008783.

Shettle, E. P., M. T. DeLand, G. E. Thomas, and J. J. Olivero (2009), Long term variations in the frequency of polar mesospheric clouds in the Northern Hemisphere from SBUV, *Geophys. Res. Lett.*, *36*, L02803, doi:10.1029/2008GL036048.

Sica, R. J., et al. (2008), Validation of the Atmospheric Chemistry Experiment (ACE) version 2.2 temperature using ground-based and space-borne measurements, *Atmos. Chem. Phys.*, *8*, 35–62.

States, R. J., and C. S. Gardner (1999), Thermal structure of the mesopause region (80–105 km) at 40°N latitude. Part I: Seasonal variations, *J. Atmos. Sci.*, *57*, 66–77.

Stevens, M. H., C. R. Englert, M. T. DeLand, and S. M. Bailey (2007), Polar mesospheric cloud mass and the ice budget: 2. Application to satellite data sets, *J. Geophys. Res.*, *112*, D08205, doi:10.1029/2006JD007532.

Stevens, M. H., et al. (2010), Tidally induced variations of polar mesospheric cloud altitudes and ice water content using a data assimilation system, *J. Geophys. Res.*, *115*, D18209, doi:10.1029/2009JD013225.

Summers, M. E., R. R. Conway, C. R. Englert, D. E. Siskind, M. J. McHugh, M. H. Stevens, J. M. Russell, L. L. Gordley, and M. J. McHugh (2001), Discovery of a water vapor layer in the Arctic summer mesosphere: Implications for polar mesospheric clouds, *Geophys. Res. Lett.*, *28*, 3601–3604, doi:10.1029/2001GL013217.

Thomas, G. E. (1984), Solar Mesospheric Explorer measurements of polar mesospheric clouds noctilucent clouds, *J. Atmos. Terr. Phys.*, *46*, 819–824, doi:10.1016/0021-9169(84)90062-X.

Thomas, G. E. (2003), Are noctilucent clouds harbingers of global change in the middle atmosphere?, *Adv. Space Res.*, *32*, 1737–1746, doi:10.1016/S0273-1177(03)90470-4.

von Zahn, U., and U. Berger (2003), Persistent ice cloud in the midsummer upper mesosphere at high latitudes: Three-dimensional modeling and cloud interactions with the ambient water vapor, *J. Geophys. Res.*, *108*(D7), 8451, doi:10.1029/2002JD002409.

von Zahn, U., J. Höffner, V. Eska, and M. Alpers (1996), The mesopause altitude: Only two distinctive levels worldwide?, *Geophys. Res. Lett.*, *23*(22), 3231–3234, doi:10.1029/96GL03041.

von Zahn, U., G. Baumgarten, U. Berger, J. Fiedler, and P. Hartogh (2004), Noctilucent clouds and the mesospheric water vapour: The past decade, *Atmos. Chem. Phys.*, *4*, 2449–2464, doi:10.5194/acp-4-2449-2004.

Waters, J. W., et al. (2006), The Earth Observing System Microwave Limb Sounder (EOS MLS) on the Aura satellite, *IEEE Trans. Geosci. Remote Sens.*, *44*(5), 1075–1092, doi:10.1109/TGRS.2006.873771.

S. M. Bailey, Bradley Department of Electrical and Computer Engineering, Virginia Polytechnic Institute and State University, Blacksburg, VA 24061, USA.

M. E. Hervig, GATS Inc., Driggs, ID 83422, USA.

P. P. Rong and J. M. Russell III, Center for Atmospheric Sciences, Hampton University, Hampton, VA 23668, USA. (ping-ping.rong@hamptonu.edu)